Paper ID ILASS08-9-1

ILASS 2008
Sep. 8-10, 2008, Como Lake Italy

SIMULATIONS OF DROPLET IMPACT ON COLD WALL WITHOUT WETTING

Norbert Roth, Jan Schlottke, Juliane Urban and Bernhard Weigand

Institut für Thermodynamik der Luft- und Raumfahrt (ITLR)
Universität Stuttgart
Pfaffenwaldring 31
D-70550 Stuttgart, Germany
e-mail: norbert.roth@itlr.uni-stuttgart.de

ABSTRACT

Simulations of droplets impacting on walls with ambient temperature have been performed. For the simulations the in-house code FS3D has been used. It solves the incompressible Navier-Stokes equations. In order to describe the free surface of the droplets the Volume-Of-Fluid (VOF) method is used. The simulations have been performed for different impact angles α. For impact angles up to $\alpha = 6°$ the obtained results seem to be reliable in comparison with experimental observation performed so far. For all these cases bouncing of the droplets has been found. The deformations of the droplets have been studied as well as the air cushion which forms below the droplet during the bouncing process. The thickness of the air cushion and the pressure field directly at the wall have been studied in more detail.

1 INTRODUCTION

The impact on solid walls is one of the basic droplet dynamic processes observed in natural and technical systems like for instance raindrops impinging on the ground or droplets impacting on the walls of combustion chambers. Different wall and droplet properties are important. The wall may be rough or smooth, cold or hot, dry or already wetted by a thin liquid film. Here the focus is set on smooth dry walls. With regard to the droplet parameters its size, velocity, temperature and impact angle as well as the boiling temperature of the droplet liquid play a role for the outcomes of the impact. The impacting droplet may wet the wall or may not wet the wall just after the impact. It is well known that, for wall temperatures quite well above the Leidenfrost temperature, a thin vapour cushion is formed between droplet liquid and wall, which avoids wetting of the wall [1]. In case of such a vapour cushion the transfer of momentum and heat between droplet liquid and wall is very small in comparision to the case when the droplet is wetting the wall. For wall temperatures close to the Leidenfrost temperature different outcomes depending on the boundary conditions can be observed as reported in literature for instance in [2]. For wall temperatures below Leidenfrost temperature - even for room temperature - bouncing of impacting droplets can be observed without wetting of the wall for comparatively very small impact angles. The impact angle is defined as the angle between droplet trajectory and wall. Bouncing of droplets at cold walls has been shown in experiments performed for instance at the ITLR for ethanol droplets [3].

In the case of cold walls aerodynamic as well as hydrodynamic effects are responsible for a very thin cushion of air between the droplet liquid and wall, which avoids wetting of the wall. For higher wall temperatures evaporation processes become more and more important. In order to get more insight into the aerodynamic effects the case of a cold wall without any evaporation has been simulated numerically using the code FS3D, developed at the ITLR [4, 5]. FS3D solves the incompressible 3D Navier-Stokes equations. In order to describe free liquid surfaces the Volume-Of-Fluid (VOF) [6] method is used.

2 NUMERICS

First of all the setup of the simulations and the boundary conditions are described. Only cases with no wetting of the wall and without any heat transfer processes have been studied. Therefore the properties of the wall itself have not to be taken into account. The energy equation has not been solved. The temperature of the ambient air, the droplet, and the wall was constant at $T_0 = 293.15\,\mathrm{K}$. The properties of the droplet liquid and the ambient air are given in Table 1. In every case calculated the droplet liquid was ethanol, the droplet velocity was $v = 5\,\mathrm{m/s}$ and the droplet diameter was $D = 180\,\mu\mathrm{m}$.

Table 1. Properties of the droplet liquid (ethanol) and the ambient air, which have been used for all simulations.

Fluid		Ethanol	Air
Temperature	[K]	293.15	293.15
Density	[kg/m^3]	788.5	1.20464
Viscosity	[10^3 Ns/m^2]	1.18	0.01837
Surface tension	[10^3 N/m]	22.5	-

The geometric arrangement for the simulations is shown schematically in Fig. 1. The plane C can be defined by the trajectory of the incoming droplets and by the trajectory of the reflected droplets. This plane is naturally perpendicular to the wall. The intersection of this plane with the wall defines the x-direction. The z-direction is perpendicular to plane C and the y-direction is perpendicular to the wall. The bottom of the computational domain is the wall. The origin of the x, y, z-axes is in one corner of the block-shaped computational domain, the edges of the computational domain are oriented along the x-,y- and z-axis, respectively, as can be seen from Fig. 1. Plane C cuts the computational domain into halves. The width of the computational domain in x-direction $g_x = 600\,\mu\mathrm{m}$, in y-direction (height)

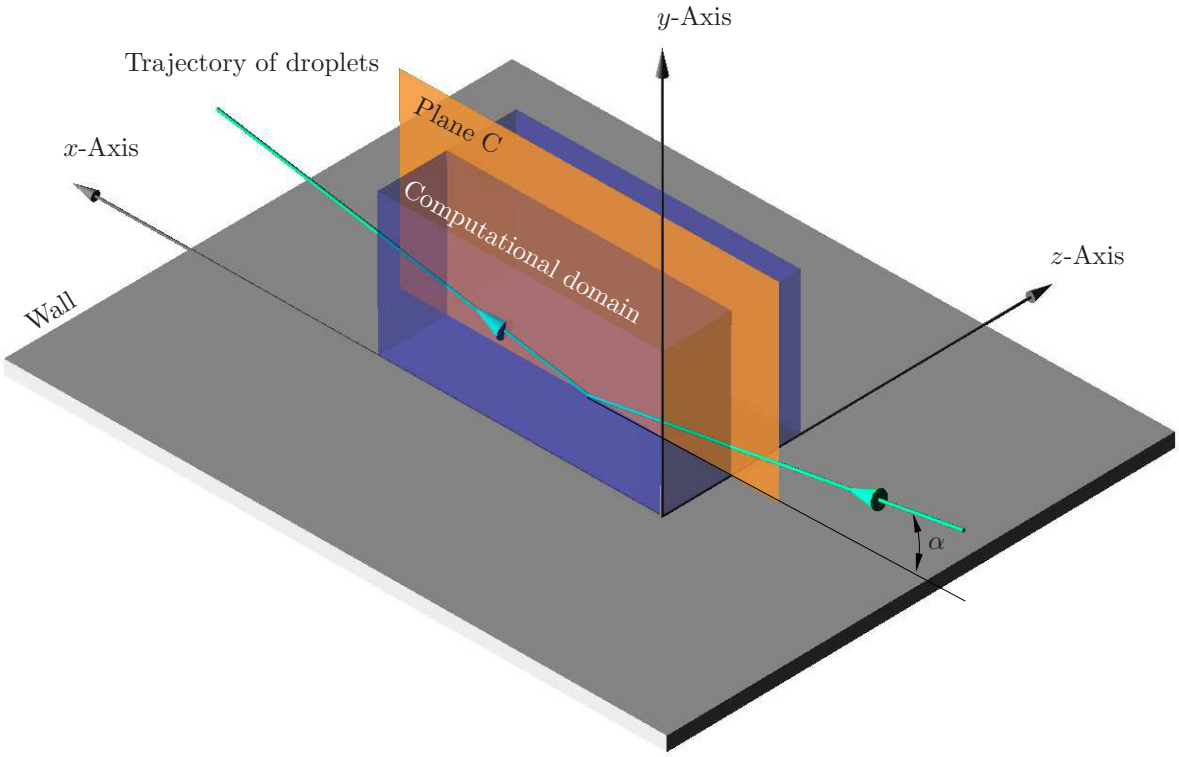

Figure 1. Schematic view of the geometric arrangement used for the simulations including the computational domain, the trajectory of the droplets and the impact angle α.

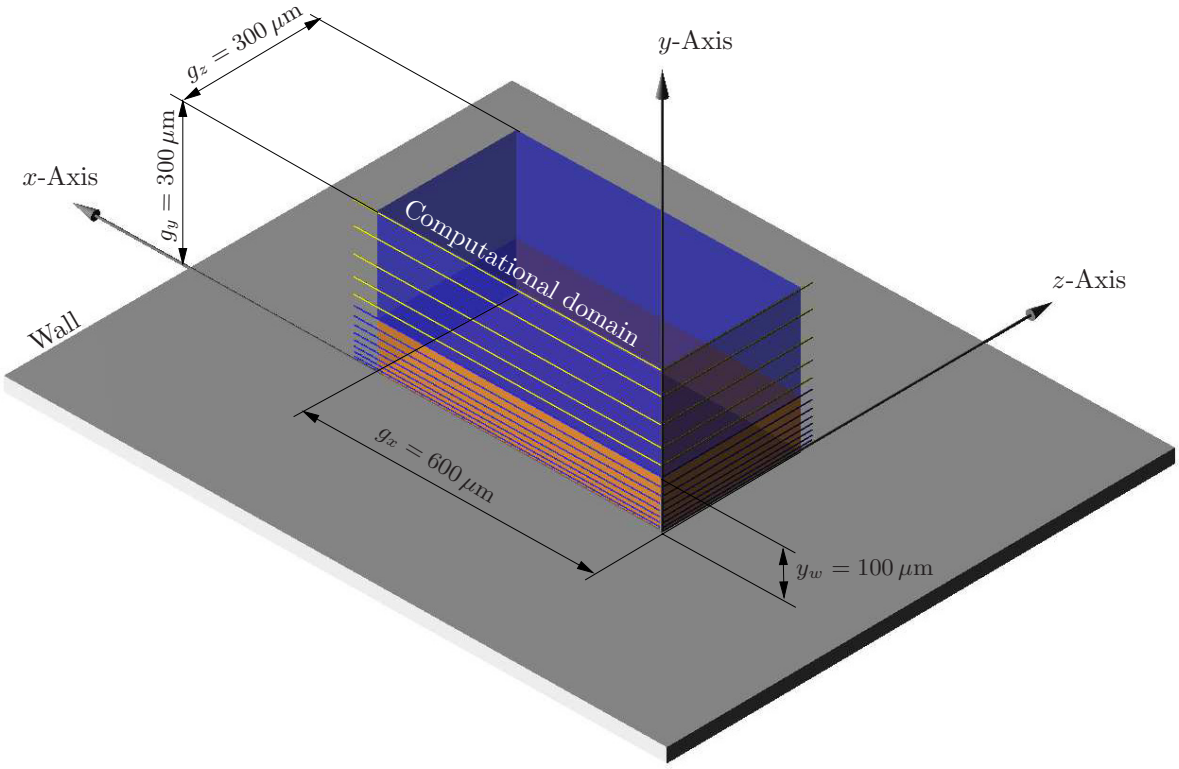

Figure 2. Sketch indicating the size of the computational domain and the grid refinement in y-direction near the wall. The position of every nth layer of grid cells in the x, z-plane is marked.

and z-direction (depth) $g_y = g_z = 300\,\mu$m for all calculations shown here. The boundary conditions have been set as follows for all simulations. At the bottom of the computational domain, which represents the wall, the condition for a wall with no slip has been set. For the other three sides of the computational domain, which are parallel to the x-direction the Neumann boundary condition has been set. It should be emphasized, that it has been payed attention to, that during the boucing process no liquid mass passes these three boundaries. For the remaining sides perpendicular to the x-direction periodic boundary conditions have been used. As a result liquid mass leaving the computational domain at $x = gx$ will immediately enter the computational domain at $x = 0$. This can be interpreted as the simulation of a monodisperse droplet stream impaction on a solid wall. The spacing between the droplets would be $d_s = gx$. Therefore these simulation can be compared easily with experiments of droplet streams impacting on cold solid walls [3].
Calculations have been performed for different grid resolutions and different impact angles. The impact angle α is defined as the angle between the trajectory of the incoming droplets and the wall.

3 RESULTS

Simulations for impact angles of $\alpha = 2°$ up to $12°$ have been performed. The results depend on the resolution of the calculation grid to some extend. Therefore in the next section it is outlined how far the grid resolution is essential. In the following section reliable results are presented and explained in detail.

3.1 Influence of grid resolution

The simulations have been performed fully 3D without any assumptions of symmetry. A rectangular grid has been used with refinements near the wall. In x-direction and in z-direction the size Δx or Δz (width or depth) of the grid cells is equidistant and can easily be calculated from the size of the computional domain (g_x, g_z) and the number of grid cells n_x or n_z, respectively. As mentioned above the vertical size of the grid cells becomes smaller near the wall. The computational domain is divided in y-direction in two sections: a lower section for $0 < y < y_w$ with n_{yl} grid cells and an upper section for $y_w < y < g_y$ with n_{yu} grid cells. The total number of grid cells in y-direction is $n_y = n_{yl} + n_{yu}$. For all cases studied the lower section was $y_w = 100\,\mu$m high. This is illustrated in Fig. 2 by indicating both sections and in addition each nth position of grid cells in y-direction. The plane with the smallest grid cells is located directly at the wall with the height $\Delta y(1)$. For increasing y-values the height of the grid cells increases. The difference in height between neighbouring grid cells is constant, however, this constant value differs between the lower and upper section. In the upper section the smallest height of the grid cells at $y(n_{yl}+1)$ equals the height of the grid cells at $y(n_{yl})$.
In this study the focus was set on the physical phenomena, not on exact values of the process. Therefore only some basic checks have been conducted. Four different configurations of the numerical grid have been used. The parameters of these resolutions can be found in Table 2.

Table 2. Overview over the grid configurations used in the simulations presented.

Grid	n_x x n_y x n_z	n_{yl}	n_{yu}	$\Delta y(1)$ [μm]	$\Delta y(n_{yl})$ [μm]
A	128 x 128 x 64	80	48	0.6250	1.850
B	256 x 256 x 128	160	96	0.3125	0.925
C	256 x 128 x 128	80	48	0.6250	1.850
D	256 x 128 x 128	80	48	0.3125	1.850

First the impact angle $\alpha = 2°$ has been studied for two different grid resolutions A and B. In each direction grid B has twice as much grid cells as grid A. For both grid configurations and the impact angle $\alpha = 2°$ bouncing has been observed. After the comparison of various outcomes from both simulations no essential difference has been found.
For further simulations only grid C and grid D have been used. There is only one difference between both grids, namely the height of the grid cells in the lower section of the computational domain for $y < y_w$. For both configurations the height of the grid cells at the top of the lower section $\Delta y(n_{yl}) = 1.85\,\mu$m was the same. However, the height of the grid cells at the bottom of the lower section (at the wall) differs. For grid configuration C this height is $\Delta y(1) = 0.625\,\mu$m and for grid configuration D it is $\Delta y(1) = 0.3125\,\mu$m. As a result the grid resolution directly at the wall for grid D is approximately twice as high as for grid C.
Simulations for impact angles from $\alpha = 2°$ up to $\alpha = 12°$ have been conducted. First grid configuration C with the lower grid resolution at the wall has been used for impact angles $\alpha = 2°$, $4°$ and $6°$. For $\alpha = 2°$ and $4°$ bouncing of the droplets has been observed. These outcomes are realistic. However, for $\alpha = 6°$ the droplet liquid wets the wall. This seems not to be realistic, as in former experiments performed at the ITLR bouncing for impact angles $5° < \alpha < 6°$ has been observed. In order to test if the grid resolution influences the outcomes grid configuration D with a higher grid resolution near the wall has been used for impact angles $\alpha \geq 6°$.
Following results have been obtained. For $\alpha = 6°$ now bouncing has been obtained. For $\alpha = 8°$ similar results as for $\alpha = 6°$ have been obtained, however, larger angles have not been studied in the experiments until now. For $\alpha = 10°$ a strong deformation in x-direction is detected, which may be realistic due to friction effects. For $\alpha = 12°$ wetting of the wall has been observed.
It is clear, that for higher impact angles wetting of the cold wall must be observed. However, to determine from simulations the limit of the impact angle, at which wetting occurs, is at least very difficult if not impossible. In order to overcome this problem or to obtain more insight into the physics, comparisons with experiments are necessary. A further refinement of the grid near the wall is difficult as Knudsen number effects, which are not taken into account yet, may then play an increasing role.
Table 3 gives an overview over the results of the simulations performed.
In the following section the dynamic behaviour of the impact process is presented for simulations, which are supposed to be realistic. These are printed in Table 3 in bold face.

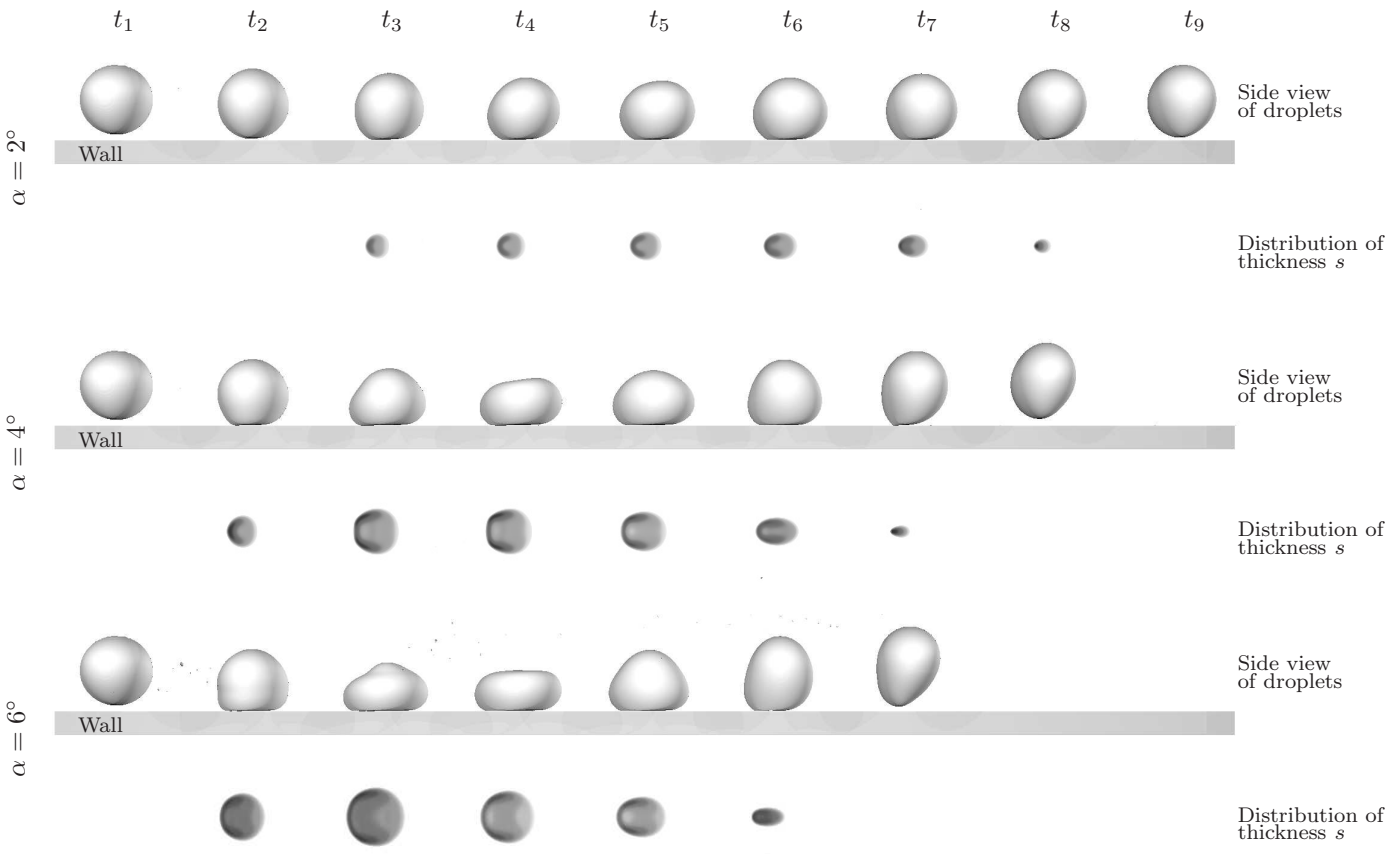

Figure 3. Results of simulations of a droplet impacting on a wall. Shown are results during bouncing process at nine different times t_i and for three different impact angles α. For each angle the upper line shows the droplet deformations qualitatively; in the lower line each picture shows the corresponding pictures indicating the thickness s of the air cushion below the droplet. The gray levels indicate the values of thickness s. Totally black (not reached for bouncing) means the wall is wetted. Totally white means the distance is $s \geq 3\,\mu$m.

Table 3. Overview over all simulations mentioned above. Those cases presented in more detail are printed in bold face.

α	Grid	Result
2°	*A*	Bouncing
2°	*B*	Bouncing
2°	**C**	**Bouncing**
4°	**C**	**Bouncing**
6°	*C*	Wetting
6°	**D**	**Bouncing**
8°	*D*	Bouncing
10°	*D*	Bouncing
12°	*D*	Wetting

3.2 Dynamic behaviour

Different parameters characterize the dynamic behaviour of the droplet impact on a cold wall with bouncing of the droplet. Obviously the droplet deformation during the impact process is of interest. Essential, however, is the droplet behaviour close to the wall. Interesting parameters are the thickness of the air cushion below the droplet and the pressure distribution directly at the wall especially below the droplet. For future investigations and practical applications heat transfer processes are very important.
The droplet deformation during the droplet impact can be seen qualitatively from Fig. 3 for three different impact angles. In the upper part for every angle the droplets are shown from the side at nine different times. The deformation for larger impact angles is stronger as expected. The deformation looks quite realistic in comparison with experiments performed [3]. A direct comparison with these experiments is not possible due to the difference of the initial parameters. A measure for the degree of deformation is the area A of the free liquid surface in comparison with the free liquid surface area A_0 of the spherical droplet. The development of the ratio A/A_0 during the impact process

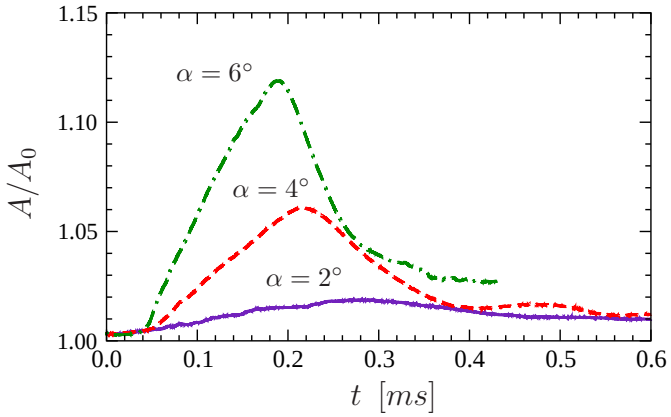

Figure 4. Ratio A/A_0 of the free liquid surfaces as a fuction of time t for three different impact angles characterizing the deformation of the droplet during the impact process.

is shown in Fig. 4 for three different impact angles. As the droplet is not spherical after the impact process and it will oscillate the value for a spherical droplet is not recovered. It can be seen again, that for increasing impact angle the surface area increases.
For the bouncing process the conditions near or directly at the wall are important. From the simulations the thickness s, indicated in Fig. 5, of the air cushion below the droplet can be obtained. In Fig. 3 corresponding distributions

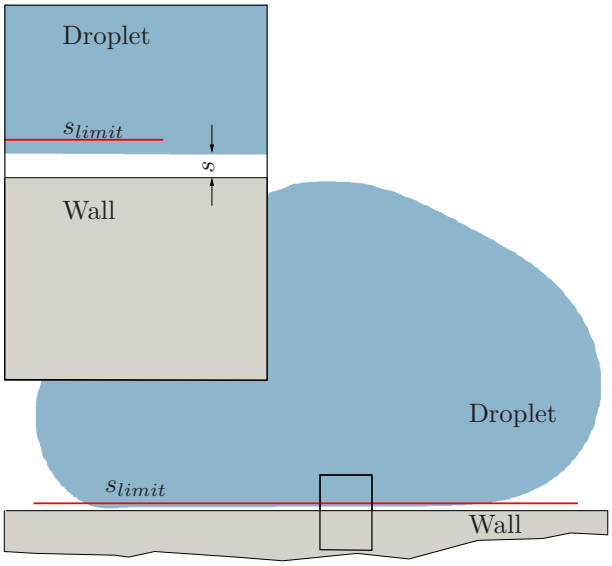

Figure 5. Intersection at plane C through a bouncing droplet. In the enlarged view the thickness s of the air cushion below the droplet is indicated in addition with the height s_{limit} of the level below the thickness s is depicted in Fig. 3.

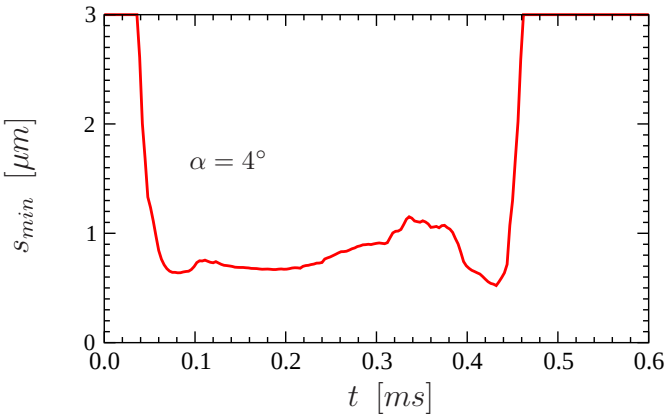

Figure 6. Minimum s_{min} of the thickness s as a function of time t for $\alpha = 4°$.

of s are depicted in addition. The gray levels indicate the values of s. The darker the color the smaller is s. Above $s = s_{limit} = 3\,\mu$m the picture is white. It can be seen that for the ongoing bouncing process the area for which $s \leq s_{limit}$ increases, reaches a maximum and decreases until the droplets lifts off from the wall. In Fig. 6 the minimum s_{min} of the spacing is shown as a function of time for the case $\alpha = 4°$, which has been simulated with grid C. At the beginning of the impact process a local minimum of s_{min} can be found. Then s_{min} increases and astonishingly it decreases again at the end of the bouncing process forming a local minimum just before the lift off of the droplet.
Concerning the thickness s the focus was until now on the temporal evolution. The distribution of s at a given time can be analyzed in detail from Fig. 7. Shown in this figure

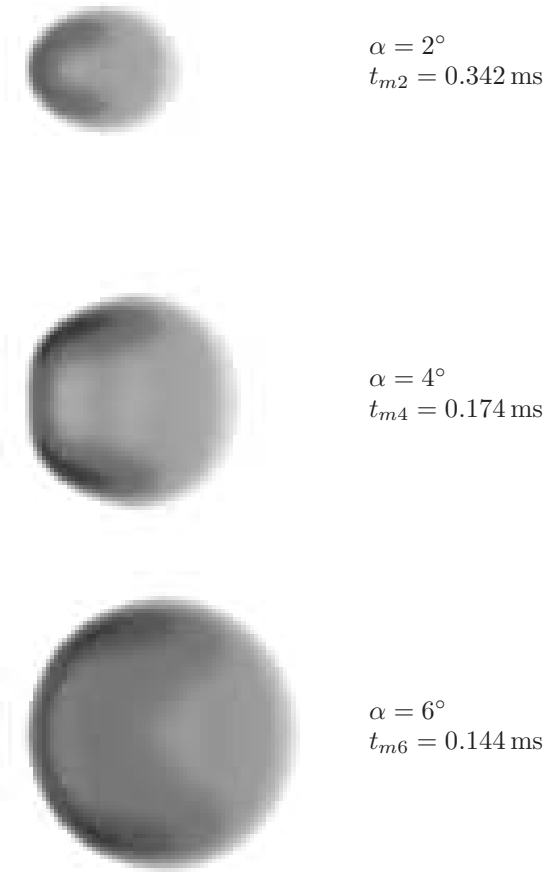

Figure 7. Distribution of thickness s of the air cushion below the droplet at three different times. The gray levels indicate the values of the thickness. The spacing is a function of the position x, z on the wall. Totally black (not reached for bouncing) means the wall is wetted. Totally white means the distance is $s \geq s_{limit} = 3\,\mu$m. The droplets move from left to right. Shown are results for three different impact angles α.

are similar pictures as shown in Fig. 3 at times, which are before the maximum values of A/A_0 are reached. The motion of the droplet is from left to right. For all impact angles shown, a symmetric distribution can be found. In the front region the spacing is larger, whereas in the backward region for all cases a relatively sharp horse shoe shaped region with small thicknesses can be found. However, for $\alpha = 4°$ there seems to be a gap in the middle of the horse shoe shaped region. If this gap and its disappearance for larger impact angles is realistic will be investigated in future. In order to give quantitative results in Fig. 8 the thickness s is shown along the middle axis, which is the intersection of plane C with the wall. Shown is the region below the droplet for the distributions of Fig. 7. The

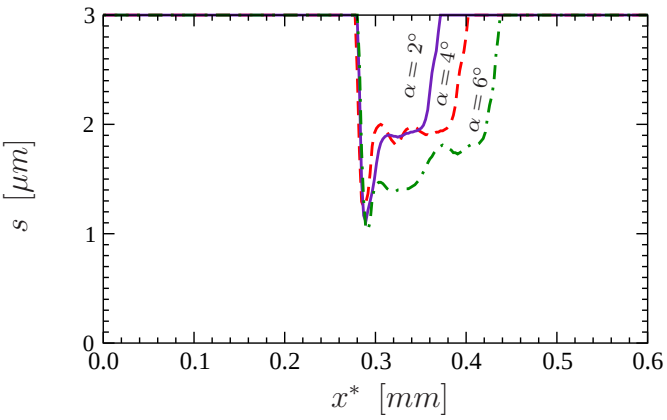

Figure 8. Thickness s of the air cushion below the droplet along the center line defined by the intersection of plane C and the wall for three different impact angles α. Used grids are those in bold face given in Table 3.

minimum of s is at the location of the horse shoe shaped region for all three cases. For $\alpha = 4°$ and $6°$ there seem to exist capillary waves in the front region (with respect to the droplet motion).

The pressure field below the droplet can give a deeper insight in the phenomena observed during the bouncing process. In order to gain a feeling of the flow below the droplet pathlines at the wall are shown in Fig. 9 assuming that the observer is moving with the initial velocity $\vec{v}_0$ of the droplet. In addition the wall and the droplet are depicted.

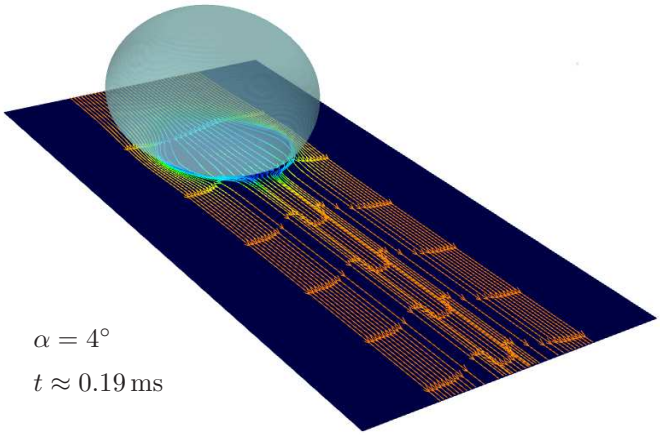

Figure 9. Flow field near the wall for the case of $\alpha = 4°$. Shown are the pathlines obtained for an observer moving with the droplet, the wall and the droplet itself.

Shown is the case with $\alpha = 4°$. The gap in the horse shoe shaped clearly can be recognized in the behaviour of the streamlines. The pressure field directly at the wall is presented in Fig. 10 for the three cases with $\alpha = 2°$, $4°$ and $6°$. Shown is the pressure difference Δp with respect to the regions, which are not influenced by the droplet. The pictures have to be compared with Fig. 7. The droplets are moving away from the observer, that means in positive x-direction. The times at which the situation is shown are the same for each case as the times used in Fig. 7. In addition the droplet is depicted. Far away from the droplet the pressure difference is zero (yellow region). The pressure field looks very similar to the distribution of the spacing s shown in Fig. 7. Here again a horse shoe shaped region can be identified. The pressure difference Δp in this region is negative (depicted in blue), therefore the droplet liquid is sucked towards the wall. In the regions below the droplet, but outside of the horse shoe shaped region, Δp is positve (depicted in red). In these regions the droplet liquid is pushed away from the wall. There is a very sharp pressure drop between the two regions with positive and negative Δp. This can be seen more clearly in Fig. 11. In this figure the pressure difference Δp is shown along the center line defined by the intersection of plane C and the wall. Shown is the result for $\alpha = 4°$ in the region of the

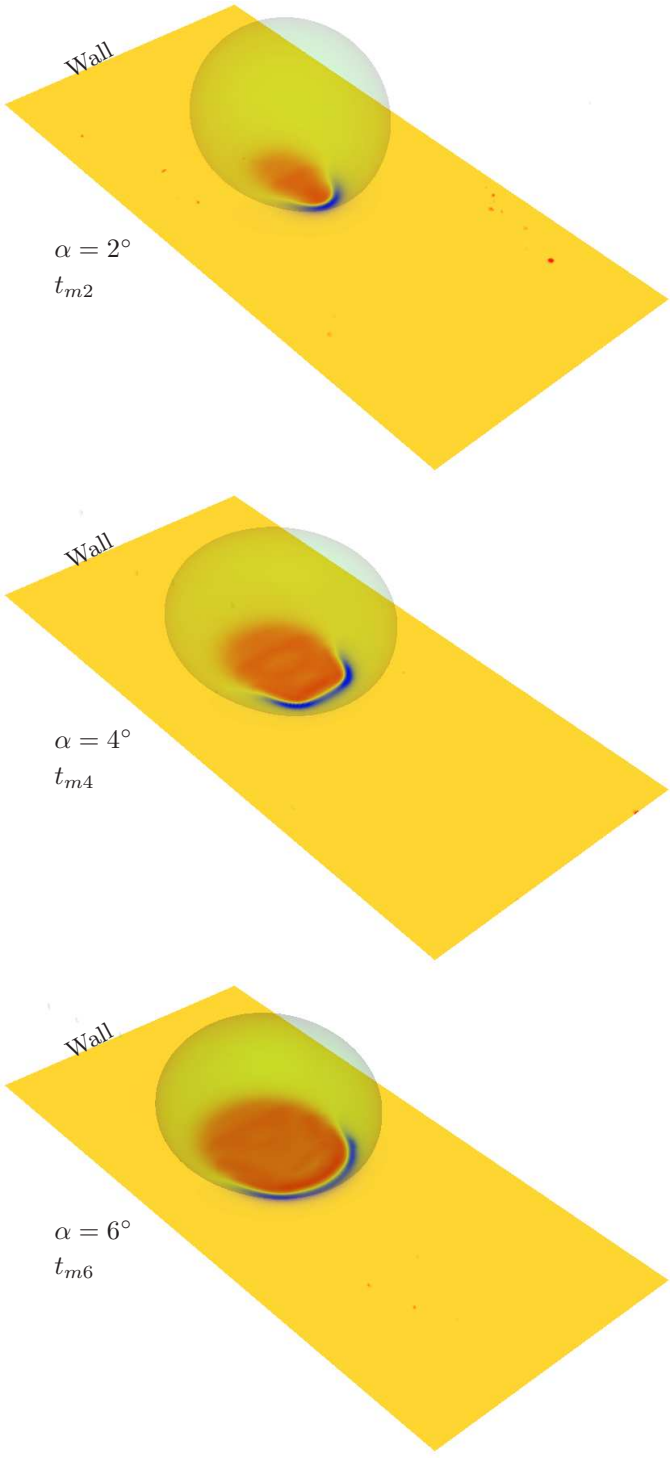

Figure 10. Distribution of the pressure difference Δp at the wall with respect to the regions, which are not influenced by the droplet for three different impact angles. In addition the droplet is shown.

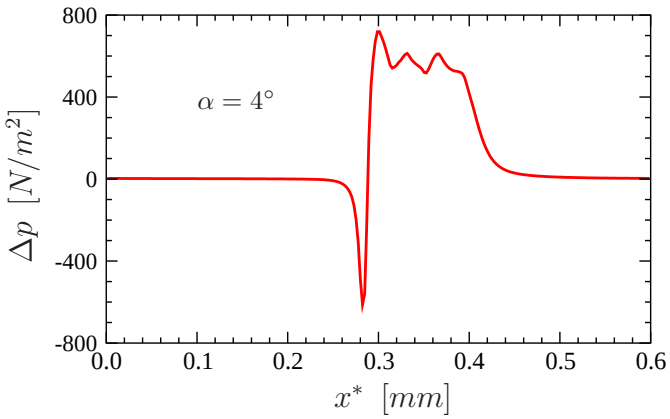

Figure 11. Pressure difference Δp along the center line defined by the intersection of Plane C and the wall at time t_{m2} for $\alpha = 4°$.

droplet at time t_{m2}.

4 CONCLUSION, OUTLOOK

Simulations of the impact of droplets on a cold wall have been performed. Some investigations have been made concerning the grid resolution. As results cases are presented which are plausible in comparison with experiments performed at the ITLR. It has been found that: the larger the impact angle the larger the deformation of the droplet and the larger the region A_s of air cushion below the droplet, which forms when the droplet approaches the wall. The thickness s of the air cushion below the droplet, that means the spacing between droplet liquid and wall, is not constant with time. At any time the thickness s has a non-constant distribution below the droplet. A horse shoe shaped region with lower values of the thickness can be identified at the trailing edge of the air cushion. In this region the pressure of the air is lower than far away from the droplet. In the other regions of the air cushion the pressure is higher. This means that the droplet liquid is sucked to the wall in the horse shoe shaped region at the trailing edge and the droplet liquid is pushed away from the wall in the other regions of the air cushion.

In future work the influence of the pressure distribution below the droplet on the bouncing or wetting behaviour will be studied. In order to compare directly experiments with simulations with the same initial parameters an experimental setup has been build up and first experiments have been performed.
Next steps for the simulations of droplet-wall interaction will be the impact on hot walls including evaporation processes. These features have already been implemented in the in-house code FS3D.

References

[1] N. Roth, T. Straub, and B. Weigand. Observation method to obtain information on the vapour film during the collision of droplets with hot walls. In *Proc. 9th Int. Conf. on Liquid Atomization and Spray Systems*. ICLASS, 2003.

[2] G.E. Cossali, M. Marengo, and M. Santini. Multiple drop impact on heated surface. In *Proc. 9th Int. Conf. on Liquid Atomization and Spray Systems*. ICLASS, 2003.

[3] N. Roth, A. Karl, and A. Frohn. Observation of liquid-wall contact during droplet impact. In *Proc. 14th Int. Conf. on Liquid Atomization and Spray Systems*, pp. 103–107, Manchester, England, 1998. ILASS.

[4] M. Rieber. *Numerische Modellierung der Dynamik freier Grenzflächen in Zweiphasenströmungen*. PhD Thesis, Universität Stuttgart, 2004.

[5] M. Hase. *Numerische Berechnung dreidimensionaler Transportvorgänge an angeströmten, sich verformenden Tropfen*. PhD Thesis, Universität Stuttgart, Shaker-Verlag, 2005.

[6] C.W. Hirt and B.D. Nichols. Volume of fluid (VOF) method for the dynamics of free boundaries. *J. Comput. Phys.*, Vol. 39, pp. 201–225, 1981.